JACS
JOURNAL OF THE AMERICAN CHEMICAL SOCIETY

ARTICLE

pubs.acs.org/JACS

Mixed Dithiolate Durene-DT and Monothiolate Phenylethanethiolate Protected Au_{130} Nanoparticles with Discrete Core and Core-Ligand Energy States

Zhenghua Tang, Donald A. Robinson, Nadia Bokossa, Bin Xu, Siming Wang, and Gangli Wang*

Department of Chemistry, Georgia State University, Atlanta, Georgia 30302, United States

Supporting Information

ABSTRACT: A new type of gold nanoparticle with interesting energetics has been created by employing a mixture of dithiol durene (Durene-DT) and monothiol phenylethanethiol (PhC2S) in the synthesis. The average composition of these mixed thiolate clusters is characterized to be $Au_{130}(Durene\text{-}DT)_{29}(PhC2S)_{22}$. Continuous quantized core charging behaviors were observed at lower potentials in voltammetric measurements, while ligand reaction and core-ligand interactions were observed at higher potentials. The absorbance spectrum displays discrete absorption bands at ca. 355, 490, 584, and 718 nm. The electrochemical and absorbance features are correlated through the determined energy states and charging energy. Broad near-IR luminescence was observed, associated with significant relaxation of excitation energy. Such interesting optical and electrochemical properties are attributed to the nanoparticle core size, ligand composition, and core-ligand charge delocalization determined by the dithiolate molecular structure.

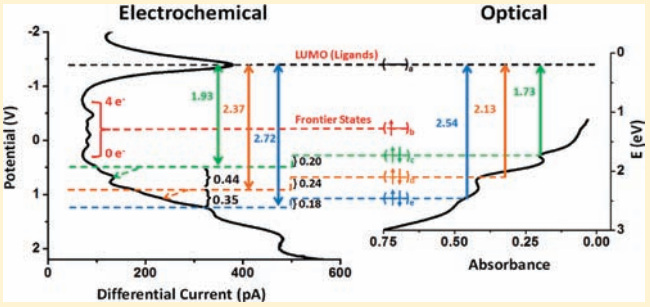

INTRODUCTION

Small gold nanoparticles stabilized by thiolates, often referred as monolayer protected clusters (MPC), have attracted extensive research interests due to their rich optical, electrochemical, and other physiochemical properties.[1−3] Those fundamental properties, together with their favorable small dimension and nontoxic chemical components, lead to broad applications in biomedicine, sensing, optoelectronics, and catalysis.[3−6] Breakthroughs have been achieved recently in the composition and structure elucidation of AuMPCs at atomic and molecular level, including $Au_{25}(SR)_{18}$, $Au_{38}(SR)_{24}$, and $Au_{102}(SR)_{44}$ by X-ray crystallographic studies[7−11] and theoretical calculations.[12−15] A novel interfacial bond structure, the RS-Au-SR "staple" motif, has been discovered in the form of single or extended units (e.g., RS-Au-SR-Au-SR), coping with different core surface curvatures.[7−16] Superatom theory has been proposed, through which the underlying electronic structure corresponding to the absorbance features of these molecular gold clusters has been theoretically described.[17]

Nanomaterials with desired physiochemical properties are needed for targeted applications. It is important to correlate the composition and structure of the nanoclusters with their properties for application design. Toward that aim, extensive research efforts have been devoted to control the size, composition, and shape of nanomaterials.[1−3] With the recent discovery of the "staple" motif at core-ligand interface of the Au MPCs,[7−10] interfacial bonding structures are believed to play an important role in the properties of nanoclusters, in addition to the well-known quantum confinement factors such as shape and size/composition.[18] Dithiolate-protected Au nanoclusters with 2,3-dimercaptopropane-1-sulfonate (DMPS, a 1,2-dithiol ligand) have been created.[18]

The Au−S bond formation with multidentate dithiols is determined by two factors: the structural constraint imposed on the surface bond formation by two thiol groups of one dithiol molecule, and the entropy gain of one dithiol over two monothiol molecules upon binding to gold. The favored composition and structure, in turn, affect the physical properties of the gold nanoclusters. The chemical reactivity, specifically the monolayer reactions between monothiol and dithiol molecules, has been explored.[19] The near IR luminescence is correlated to nanocluster composition and Au−thiolate interactions.[19] Dithiols and other multithiol ligands have also been employed in the stabilization of larger Au nanoparticles,[20−22] in the synthesis of Ag nanoclusters,[23] and targeted biointeractions.[24−26] Interesting phase segregation has been observed from the Au clusters stabilized by mixed monothiols of different polarities.[27,28] To the best of our knowledge, heterogeneous monothiolate and dithiolate ligands have not been employed in the nanocluster synthesis.

In this paper, a new type of molecular gold nanocluster is created by employing mixed aromatic thiols, monothiol ligand phenylethanethiol (PhC2S) and dithiol ligand durene-α1, α2-dithiol (Durene-DT, a 1,4-dithiol). The impacts of dithiol

Received: April 27, 2011
Published: September 16, 2011

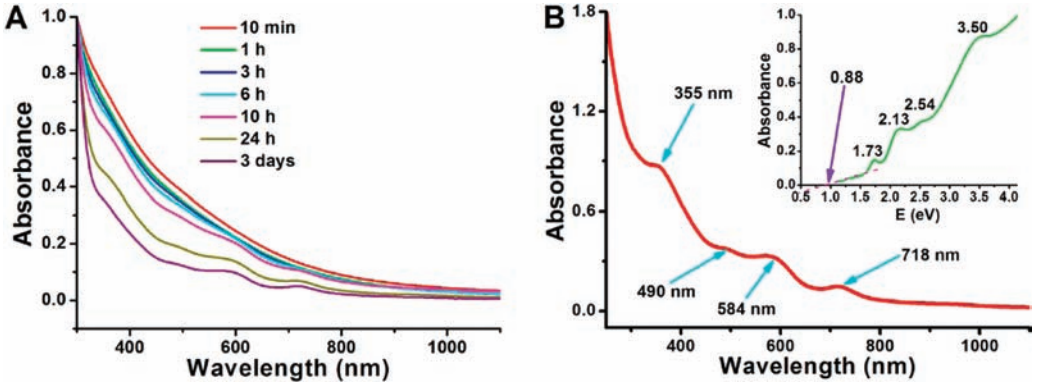

Figure 1. (A) The absorbance change during the reduction. An aliquot of the reaction mixture in toluene phase was diluted to proper absorbance range for each measurement. The spectra were normalized at 300 nm. (B) Absorbance spectrum of the purified product in methylene chloride. The spectrum plotted in energy axis is inserted.

molecular structure and dithiol/monothiol/Au ratio on the cluster formation and properties are studied. The rationale is that the dithiols preferentially bind to Au due to entropy gain.[29,30] Meanwhile, monothiols fill into those sites inaccessible by the dithiols due to molecular structure constraint and core surface curvature. The mixed thiolate clusters (MTCs) display discrete absorption bands and rich electrochemical properties. Near-IR luminescence is reported. The average composition is characterized as $Au_{130}(Durene\text{-}DT)_{29}(PhC2S)_{22}$ at $\pm 1-2$ resolution. An energy diagram is proposed to correlate the energetics measured by optical and electrochemical methods.

EXPERIMENTAL SECTION

Chemicals. Tetrachloroauric acid trihydrate ($HAuCl_4 \cdot 3H_2O$, >99.99% metals basis), sodium borohydride ($NaBH_4$, 99%), 2-phenylethanethiol (>99%), tetrabutylammonium perchlorate (TBAP, >99%), tetraoctylammonium bromide (TOABr, 98%), *trans*-2-[3-(4-tert-butylphenyl)-2-methyl-propenylidene]-malononitrile (DCTB, >99%), and organic solvents (HPLC grade) were used as received from Sigma-Aldrich. Durene-α1,α2-dithiol (>95%) was purchased from TCI-America.

Measurements. UV−visible absorbance spectra were recorded with a Shimadzu UV-1700 spectrophotometer. Luminescence was measured with a Horiba Jobin-Yvon Fluorolog 311 spectrometer with T channel, through which a visible PMT detector and a near-IR InGaAs detector were attached. MALDI mass spectra were acquired with ABI 4800 matrix assisted laser desorption ionization (MALDI) TOF-TOF analyzer, with DCTB as matrix. Proton NMR spectra were acquired on a Bruker Avance 400 MHz spectrometer in CD_2Cl_2. A CH instrument 700C electrochemical workstation was used in electrochemical measurements. An Agilent technologies HPLC 1200 series with multiple wavelength detector was used. X-ray Photoelectron Spectroscopy (XPS) analysis was conducted with a SSX-100 (Surface Science laboratories, Inc.) using an Al K-alpha X-ray source (1486.6 eV) with the analysis chamber pressure lower than 1×10^{-8} Torr.

Synthesis and Purification. The MTCs were synthesized via a modified two-phase Brust-Schiffrin method.[31] In a typical experiment, gold salt ($HAuCl_4 \cdot 3H_2O$) was first phase-transferred from an aqueous solution to a toluene solution with TOABr. The organic layer was separated, and then a mixed thiol solution (Durene-DT/PhC2S/Au = 1:2:1) was added in at moderate magnetic stirring. The solution color changed from gold yellow to colorless in ~30 min. Then freshly prepared $NaBH_4$ (20 equiv of gold) aqueous solution was added quickly while vigorously stirring. The solution turned black immediately. After the reaction was completed in 1−3 days monitored by absorbance transition, the organic layer was separated and washed by water 3−5 times. The solvent was removed by rotary evaporator, and the product was first precipitated by methanol, while the methanol solution was filtered away. The black solid was further rinsed with copious acetonitrile (stirring overnight) to remove the extra free ligand molecules. The leftover black solid was collected as final MTCs product.

Iodine Death Reaction[32]**.** In the NMR tube, AuMTCs were dissolved in CD_2Cl_2, and the 1D proton NMR spectrum was acquired. The MTCs were then decomposed by adding iodine, and the NMR tube was shaken vigorously for a while. The color changed from black to violet. Meanwhile, brown precipitate formed at the bottom of the tube. The proton NMR spectrum was recorded after the reaction was complete (several hours later).

RESULTS AND DISCUSSION

UV−Visible Absorbance of Mixed Thiolate Au Clusters. The formation of Au MTCs after the reduction by $NaBH_4$ was monitored by UV−visible absorbance measurements shown in Figure 1A. The absorbance of the reaction mixture displays a featureless decay upon reduction initially, for example, at 10 min. Multiple discrete absorption bands intensified over 24 h and became slightly better defined in ~3 days. The transition suggests the formation of thermodynamically favored or kinetically trapped species. Similar "size focusing" process associated with absorbance conversion was also observed in the one phase synthesis of $Au_{25}(PhC2S)_{18}$.[33,34] The final products were collected after the absorbance transition was finished in 1−3 days. The absorbance features of the purified product can be seen in Figure 1B. Four discernible bands at ca. 355 nm (3.50 eV), 490 nm (2.54 eV), 584 nm (2.13 eV), and 718 nm (1.73 eV) can be observed in the spectrum. An optical band gap of ca. 0.88 eV is extrapolated as indicated for this MTC sample.

It is well-known that various gold nanoclusters have discrete absorption bands. Au25 nanoparticle with ~1.33 eV band gap shows pronounced absorbance bands at ca. 400 nm (3.11 eV), 450 nm (2.76 eV), and 670 nm (1.86 eV).[9,35−38] Au38 nanoclusters stabilized by glutathione,[37] PhC2S, hexanethiolate, or dodecanethiolate have ~0.92 eV band gap and displays discrete absorption bands at ca. 520 nm (2.39 eV), 560 nm (2.21 eV), 620 nm (2.00 eV), 750 nm (1.66 eV), and 1050 nm (1.18 eV).[39−41] Recent reports show that the absorbance spectrum of highly monodisperse larger Au144 nanoclusters, previously considered featureless, displays absorbance bands at ca. 510 nm (2.44 eV)

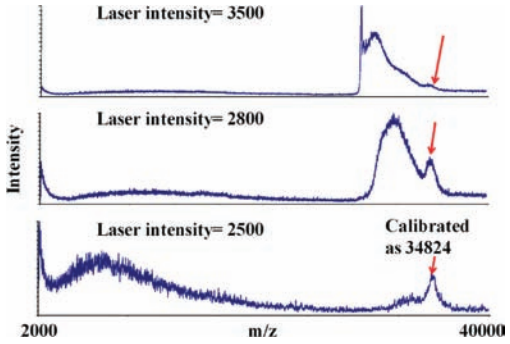

Figure 2. MALDI mass spectra of Au MTCs at different laser intensities. The spectra were collected under linear positive mode with DCTB (*trans*-2-[3-(4-tert-butylphenyl)-2-methyl-2-propenyldidene]) as matrix. No discernible signal was detected above 40000. The m/z value was calibrated with doubly charged bovine serum albumin (BSA) as external standard (Supporting Information, Figure SI-1).

and 700 nm (1.78 eV).[42] The absorbance features of the Au MTCs suggest different core size and interfacial bonding that are characterized next.

It is worth noting that the ligands employed in monothiolate AuMPC literatures do not have accessible energy states in optical absorbance and electrochemistry studies. Correspondingly, the optical bands and the electrochemical features are solely correlated with the Au core. In AuMTCs, Durene-DT (or dithiolate-Au) does have accessible states in the energy range of electrochemical and optical measurements. Analogous to the metal−ligand charge transfer process in classic inorganic complexes, core−ligand interactions induce the deviation from the size dependent trend observed in monothiol AuMPCs, which is further addressed in electrochemistry section.

Molecular Ion Identification by MALDI-MS. Since both Durene-DT and PhC2S ligands have phenyl group in their molecular structures that facilitate ionization, the MTCs were analyzed by MALDI-MS with DCTB as matrix.[43,44] The laser intensity was systematically varied to identify molecular ions. Representative mass spectra at different laser intensities under linear positive mode are presented in Figure 2. By increasing the laser intensity, a single dominant m/z peak at 34824 was identified at sufficiently low laser intensity at 2500. If the sample is a mixture of AuMTCs with multiple size/compositions, smaller MTCs should be identified at lower or comparable laser intensities. The m/z peak of 34824 is assigned to be the molecular ion species. At higher laser intensities (2800, 3500, or higher), lower m/z peaks, notably a sharp peak corresponding to mass loss of 6.11K, and broad peaks corresponding to mass loss of 5.25K and 3.09K, were observed. Because of the similar mass of Durene-DT (198) and Au (197), and linear mode used in the detection of high m/z molecular ion species, other analytical methods are necessary for the interpretation of MTC composition. Full interpretation of the fragmentation patterns and the MS analysis of MTC formation kinetics in the synthesis are under further analysis and will be separately reported.

No low m/z peaks could be detected until molecular ion species was observed. The total ion flux signal decreases as laser intensity decreases, corresponding to the higher baseline noise. An expanded view of the distorted baseline at the low m/z range (e.g., 8 kDa) at higher laser intensity is shown in Supporting Information Figure SI-2. Under negative mode, only well-defined Au_XS_Y fragment patterns were observed at low m/z range. Again,

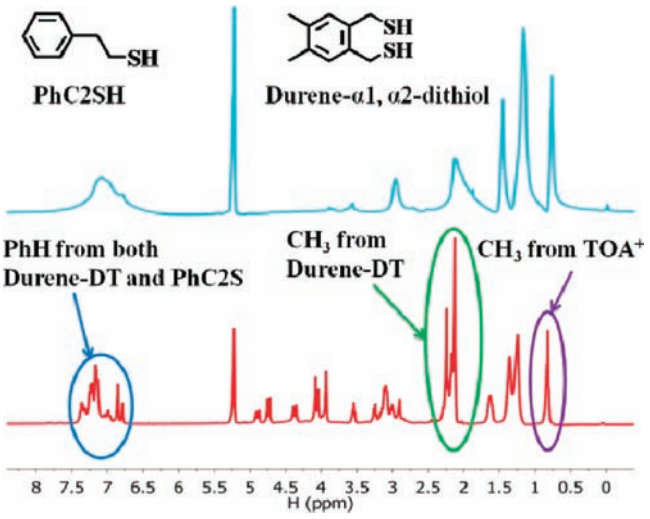

Figure 3. NMR spectra of (top) the purified MTCs and (bottom) the decomposed products. The purified MTCs (top panel) were decomposed in the same NMR tube without purification, from which the bottom spectrum was collected. The two spectra were aligned based on the sharp peak at 5.24 ppm with CD_2Cl_2 as solvent. The same figures can also be found in Supporting Information, Figure SI-6, with detailed integration included.

smaller MTCs at lower m/z range were not observed, suggesting that the proposed molecular ion species correspond to the interesting absorbance features.

The monodispersity of Au MTCs is confirmed by HPLC. Better separation was achieved after systematic variation of mobile phases (toluene and acetone, toluene and acetonitrile, chloroform and acetone) and stationary phase (phenyl, C18, and cyano column). Representative results are shown in Supporting Information, Figure SI-3. Two main peaks were consistently observed, with the dominate species accounting for ca. 80% of total sample injected. Interestingly, both species display similar absorbance features compared to the original MTC (Figure SI-4). The two eluates are believed to have the same composition but at different charge states. The assignment is further elaborated in the correlation of electrochemical and optical energetics. Similar behaviors have also been observed in the separation of Au25 nanoclusters at −1 and 0 charge states.[45] While the separation results confirm the monodispersity of the MTCs being analyzed, it is important to point out that the column materials, presumably the functional groups on unmodified silica, are known to oxidize Au nanoclusters.[46] Rest potential results before and after HPLC separation confirmed the oxidation effect, which complicates the characterization of the two species eluted (Figure SI-5).

Ligand Composition in the Monolayer Determined by ^{1}H NMR. Strong line broadening can be observed in the 1D proton NMR spectrum shown in Figure 3, a well-known effect resulting from the motion restriction and heterogeity of proton chemical environment upon cluster formation.[47] This effect suggests the presence of unbonded free ligands or smaller clusters being negligible. Otherwise, both would generate sharper features on top of the broad peaks.[48−50] The extent of the peak broadening of the purified MTCs is comparable to that observed from $Au_{144}(SR)_{60}$ MPCs (MW ca. 37K), and is much more significant than that of $Au_{25}(PhC2S)_{18}$ (MW 7.39K).[46,47,51] The observation is in agreement with the MS finding of a large nanocluster with MW at ca. 35K.

The ligand attachments on the final MTCs are analyzed by proton NMR. The phenyl proton peaks of PhC2S and Durene-DT partially overlap in the MTC spectrum, with the methyl proton from Durene-DT at ca. 2.2 ppm being the main signal readily identifiable for individual ligand species. Those methylene protons of both ligands are indiscernible in the 1D MTC spectrum due to the proximity to the Au core, therefore, significantly broadened at 2.8−5 ppm. The peak at ca. 3 ppm and those below 2 ppm indicate the presence of TOA^+, being either residue from the synthesis or part of the final MTCs as counterions addressed in the electrochemistry discussion. Note it is a well-known challenge to fully remove the TOA^+ in the synthesis and purification of AuMPCs. Furthermore, the disappearance of the thiol proton signal suggests that both thiol groups of the Durene-DT ligands bind to Au, supported by the disappearance of the thiol stretching signal in the infrared (IR) spectrum (Figure SI-7).

The mass differences of Durene-DT and Au could not be resolved by MALDI MS under linear mode. To quantify the mole ratio of Durene-DT and PhC2S in the monolayer, the purified MTCs confirmed by the proton NMR spectrum in the top panel were decomposed by iodine death reaction.[32] The same sample was directly used to collect the bottom spectrum. The liberated Durene-DT and PhC2S, generally in the form of disulfide, display sharp NMR peaks that allow quantitative analysis. Full assignment of the proton signals based on Total Correlation NMR Spectroscopy (Figure SI-8) can be found in the Supporting Information, Figure SI-9. The methylene proton signals are complicated, especially those of Durene-DT for potential reactions elaborated in electrochemistry section. To achieve best resolution, the mole ratio of the organic components is calculated based on the integrated peak intensities of the methyl group of TOA^+ (12H), methyl group of Durene-DT (6H) and phenyl groups of PhC2S (5H). Therefore, the amount of PhC2S was calculated from the total phenyl proton intensity subtracted by the Durene-DT phenyl proton contribution, which is 1/3 of the intensity of the Durene-DT methyl group based on the proton ratio of 2:6. The calculated mole ratio of Durene-DT/PhC2S/TOA^+ is 1.0:0.76:0.14. While the amount of TOA^+ varies slightly for different samples from repeated syntheses, the ratio of the two thiols is consistent at ca. 5% uncertainty determined by the NMR peak analysis.

Diffusion Coefficient and Monodispersity Probed by Diffusion-Ordered NMR Spectroscopy (DOSY). The nanoparticle size and monodispersity are further characterized by DOSY. Two dimensional (2D) NMR techniques have been used in structural determination, surface compositional analysis, and in ligand exchange kinetic studies of Au nanoparticles.[52,53] Compared with invasive mass spectrometry and surface techniques such as transmission electron microscopy (TEM), NMR techniques directly characterize the hydrodynamic states of gold nanoparticles in solution,[54] knowledge directly relevant for biological and other applications.

The DOSY spectrum of the Au MTCs is presented in Figure 4. One group of AuMTC proton signals with the same diffusion coefficient (Log(D) at −9.5) could be found. On the basis of the diffusion coefficient of $Au_{25}(SC2Ph)_{18}$ reported previously,[18] as marked in the oval region, no signal from smaller clusters (e.g., Au25 or Au38) were detected. As additional reference points, trace amount of fast diffusing molecules are also observed at Log(D) between −8.2 and −8.8, including solvent peak (CD_2Cl_2), water, and the two types of ligands. It is interesting to notice

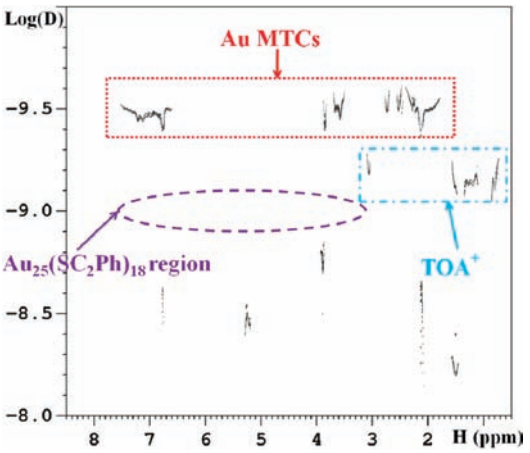

Figure 4. DOSY spectrum of Au MTCs in CD_2Cl_2 at room temperature. The x axis represents the chemical shift of the protons, while y axis is the logathrim of the calculated diffusion coefficients. The 1D spectrum can be refereed from the top panel in Figure 3.

that TOA^+ ions diffuse much slower than other small molecules. This suggests that TOA^+ ions are associated with the MTCs as counterions, which also explains its presence after extensive purification. These results attest high monodispersity of the larger MTC sample, which diffuse much slower than the well established $Au_{25}(PhC2S)_{18}$ nanoclusters.

Thermogravimetric Analysis (TGA). Because of the similarity of mass between Au and Durene-DT for MS analysis, the gold-to-organic mass ratio is determined to be ca. 70.7:29.3 by TGA (Figure SI-10). In conjunction with the mole ratio of Durene-DT/PhC2S/TOA^+ obtained from NMR analysis, the final mole ratio of Au/Durene-DT/PhC2S/TOA^+ is calculated to be 4.5:1.0:0.76:0.14. The amount of TOA^+ in different MTC samples was calculated by the respective NMR peak intensity in the composition analysis.

Molecular Composition of the Au MTCs. The "molecular formula" of these intact nanoclusters is elucidated. The molecular ion observed in MALDI-MS under positive mode is assigned to be a singly charged cationic species with one TOA^+ associated as a counterion. This argument is supported by the rest potential measurements addressed in the electrochemistry discussion. Therefore, the molecular mass at 34824 corresponds to $Au_x(Durene\text{-}DT)_y(PhC2S)_z(TOA^+)_1$. The uncertainty of TOA^+ amount observed in solution NMR measurements is not expected to affect the MS analysis, which is recorded in gas phase under ionization. The final values of x, y, and z are then calculated to be 130, 29, and 22, respectively, determined by NMR and TGA. The composition of the MTCs is proposed to be $Au_{130}(Durene\text{-}DT)_{29}(PhC2S)_{22}$, with varied charge states as characterized by rest potential measurements. Considering the measurement error associated with the techniques, specifically the NMR peak intensity integration, TGA calculation, and linear mode used due to the high mass range, the error is estimated to be at ±1−2 resolution. The comparison of those possible compositions with experimental results is summarized in Supporting Information, Table SI-1. Further computational and crystallographic studies would offer valuable knowledge of the bond structures and confirm the elucidated composition and energetics.

Near-Infrared (IR) Luminescence of Au_{130} MTCs. Broad luminescence was observed spanning from visible to near IR

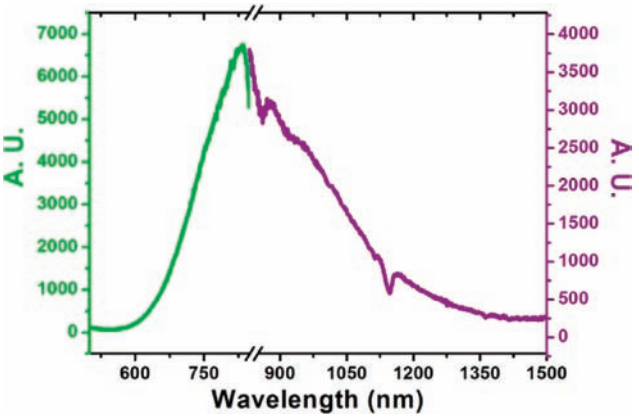

Figure 5. Luminescence of dilute Au_{130} MTCs at room temperature in CH_2Cl_2, excited at 400 nm. The left and right emission spectra were collected by the visible (up to 850 nm) and near-IR detector (from 850 nm) separately. The distortion near the break on wavelength axis is limited by the detector correction file. Individual emission spectra without correction can be found in Supporting Information, Figure SI-11.

range as shown in Figure 5. The corresponding excitation spectrum displays a broad excitation ranging from 300 to 500 nm with a maximum at ca. 400 nm (Figure SI-12). Significant energy relaxation exists between the excitation and emission maximum. The absorbance features are absent in the excitation spectrum. The luminescence properties are reminiscent of those from various AuMPCs: near-IR emission at a common energy with featureless excitation regardless of absorbance features.[55−58] The observation is attributed to the presence of Au(0) core, through which those excitons are effectively relaxed into common states defined at the Au−thiolate interface. The relaxation mechanism through Au(0) core distinguishs these nanoclusters from conventional Au(I) inorganic complexes, in which the absorbance, luminescence excitation, and emission correlate well in a similar fashion as organic dye molecules.[59,60]

In monothiol AuMPCs, luminescence quantum efficiency (QE) increases significantly (up to ca. 10^{-2}) upon the polarization of ligand monolayer and Au core, by ligand exchange reaction or by electrochemical charging.[56,61,62] Using tiopronin AuMPCs (Average composition Au_{201}(tiopronin)$_{85}$, QE at ca. 0.10%) as standard materials,[56] the quantum yield of the AuMTCs is calculated to be ca. 0.35% based on the integrated area ratio. The thiol bridging motif (RS-Au-SR) suggests the physical origin of the unique common energy states, as the Au atom embedded between the two thiolates has different chemical environments from other Au atoms. The dithiol ligands in 1,2-dithiol DMPS stabilized Au−dithiol nanoclusters have been found to impose structural constraint on the Au−thiolate bond formation and efficiently eliminate the luminescence.[18] Monolayer reactions between monothiol tiopronin and 1,2-dithiol DMPS were found to effectively switch the luminescence on and off.[18,19] The 1,4-dithiol, Durene-DT apparently has more flexible structures compared to 1,2-dithiol DMPS. The high surface coverage by Durene-DT and the presence of monothiolate PhC2S also contributed to the high QE observed from these MTCs.

Binding Energy by X-ray Photoelectron Spectroscopy (XPS) Studies. The high thiol/Au ratio is approaching the theoretical limit of full surface passivation of a packed Au core.[47] The charge

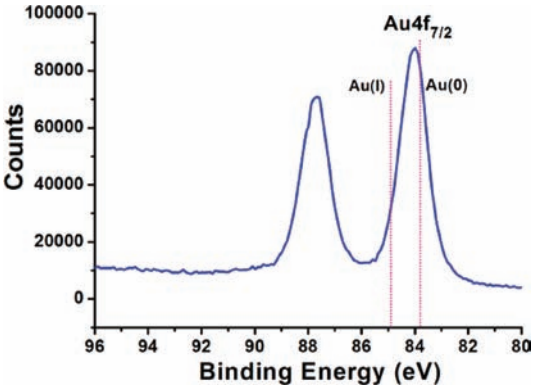

Figure 6. Au XPS spectrum of the Au_{130} MTCs. Dash lines illustrate the previously reported Au (0) and Au(I)−thiolate binding energies. The binding energy is calibrated by C (1S) at 284.6 eV shown in Figure SI-14.

states of Au and S, especially the presence of Au(0) core, are evaluated by XPS. The binding energy (BE) of Au(4f7/2) is measured to be 84.0 eV shown in Figure 6. It has been reported in AuMPC studies that the Au(4f7/2) BE increases as the particle size decreases, within the range from Au(0) film at ∼83.8 eV to Au(I) thiolate species at ca. 84.5−86.0 eV.[37,47,63,64] The BE of these Au_{130} MTCs agrees with the reported results but appears to be very close to Au(0). The observation confirms our characterization of a relatively large Au_{130} core. Among several factors previously proposed,[64] the initial charge states of the AuMTC are believed to be the main reason for the low Au(I) signal detected. The high thiolate/Au ratio, and therefore S−Au interactions in the Au MTCs, is confirmed by the S(2p) spectrum in Supporting Information, Figure SI-13. The BE of S(2p) at 162.5 eV is similar to that of Au(I) complexes and ca. 0.5 eV more positive than that from larger Au nanoparticles.[64,65] No Br or Cl signal is observed in survey scan (Figure SI-14). The XPS results confirm the presence of Au(0) core, which allow the relaxation of luminescence excitation, and the quantized charging behaviors observed in electrochemistry.

Electrochemical Properties of Au_{130} MTCs. Square wave voltammograms (SWV) shown in Figure 7 were collected at low temperature for better peak resolution at broad potential window. Cyclic voltammograms (CV) are provided in Supporting Information, Figure SI-15. Precise peak potentials were measured by differentiating the data and extrapolating the derivative plot to cross zero (Figure SI-16). Those values corresponding to the notable SWV peaks were listed in Table 1 for the calculation of electrochemical energetics. Four uniformly spaced peaks (#2−5) near zero potential were well-resolved, with the oxidation scan shown in panel B. This corresponds to four continuous quantized charging events. A differential pulse voltammogram at room temperature is provided in Supporting Information, Figure SI-17, clearly showing the regular peak spacing between each of the four peaks. The continuous quantized charging behaviors of Au_{130} MTCs are similar with those observed from large monothiol AuMPCs such as $Au_{140-147}$.[66,67]

Importantly, the electrochemical behaviors are fundamentally different from those of small monothiol AuMPCs such as Au_{25} that display electron transfer (ET) activities at discrete energy states.[2,36,40,68,69] One dominant irreversible peak at −1.4 V is observed upon reduction (note the high current in cyclic voltammogram, Figure SI-15). Free durene−dithiol molecules undergo irreversible reduction at ca. −1.6 V (Figure SI-18), corresponding to one electron reduction to the corresponding anionic

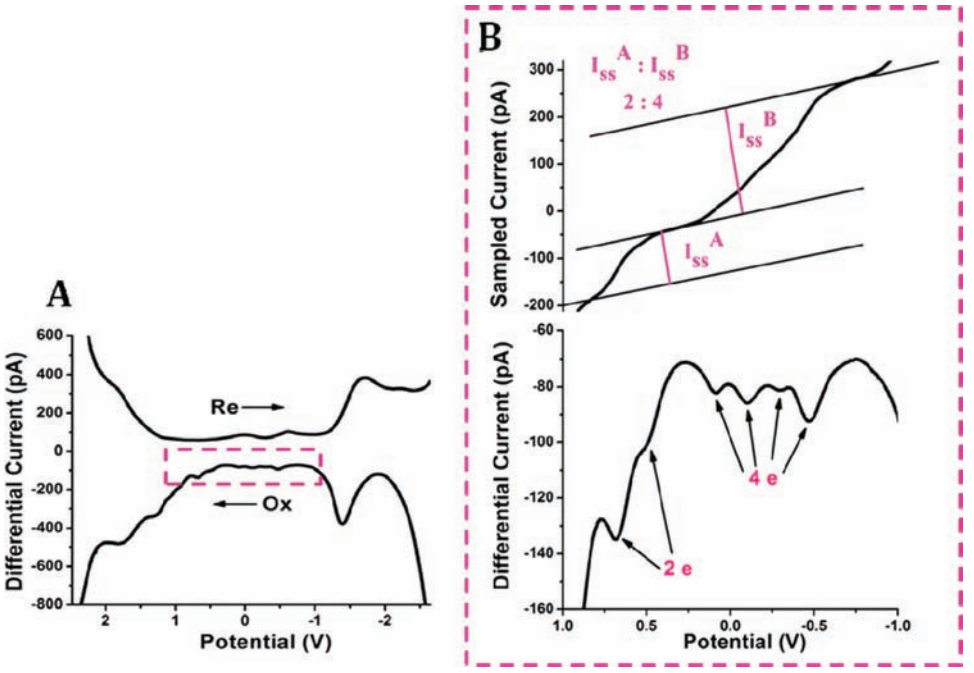

Figure 7. (A) Square wave voltammogram (SWV) of Au MTCs, recorded in 0.1 M TBAP in CH_2Cl_2 solvent at −70 °C. (B) Magnification of oxidation scan in SWV with one corresponding sampled current shown above. Step amplitude was at 25 mV with 4 mV increments. Frequency was 15 Hz. The working electrode was a 20 μm Pt disk electrode. An Ag/AgCl wire as reference electrode was calibrated in 2 mM ferrocene with 0.1 M TBAP solution prior to use. The sample solution, in CH_2Cl_2 at ca. 3 mM, was degassed under Argon prior to the measurements.

Table 1. Potential and Peak Spacing of the Au MTCs[a]

Peak #	11	10	9	8	7	6	5	4	3	2	1
Potential (V)	1.84	1.32	1.14	0.97	0.68	0.53	0.09	-0.10	-0.30	-0.47	-1.40
Peak spacing	11-10	10-9	9-8	8-7	7-6	6-5	5-4	4-3	3-2	2-1	
Energy (eV)	0.52	0.18	0.17	0.29	0.15	0.44	0.19	0.20	0.17	0.93	

[a] Data calculated from Figure 7.

radicals.[70−73] The major peak at −1.4 V is attributed to the radical formation upon reduction. The reduction potential is lower than free dithiol molecules, suggesting the stabilization by the interaction with Au core. The electron could therefore be delocalized between the Au core and the attached Durene-DT ligands. Unlike those monothiol ligands that do not have accessible energy states, the energy states of Durene-DT ligands and Au core will hybridize, leading to the quantized Au core charging at lower potentials and ligand reactions at higher potentials. To clarify, the apparent gap between major peaks in voltammogram is not from the core HOMO−LUMO energy states observed in small monothiol AuMPCs such as Au25 or Au38. Those apparent LUMO states are rather dominated by Durene-DT ligands.

The charging energy of Au_{130} MTCs is determined by the average peak spacing as 0.19 V. This value is slightly smaller than that observed in PhC2S or hexanethiolate stabilized Au25 and Au144 MPCs.[54,55,63,67] Durene-DT has one instead of two methylene groups between the Au core and phenyl group compared to PhC2S, therefore, slightly less monolayer thickness and larger dielectric constant. Furthermore, TOA^+ ions have been found to be associated with the MTCs in solution by NMR DOSY measurements. On the basis of concentric sphere model and optimization,[74] those effects will lead to smaller charging energy. Separated by a 0.44 V gap (peak # 6−5), another pair of ET peaks reveals one energy state below the frontier states. The current ratio is found to be 2:4 from one scan of the square wave data (comparable to cyclic voltammogram current). Therefore, all six differential current peaks are attributed to single electron transfer activities. The baseline distortion in sampling current prohibits similar interpretation at higher potentials/energies.

The Correlation of Electrochemical and Optical Energetics: Core Charging and Core−Ligand Charge Delocalization. In classic inorganic metal−ligand complexes, the charge transfer between metal center and stabilizing ligands is known to generate rich optical and electrochemical features. For the Au MTCs, the core−ligand interaction, analogous to those metal−ligand charge transfer effects, is found to significantly affect the energetics. Shown in Figure 8, the absorbance bands and electrochemical activities are correlated using oxidation scan that generally offers better resolved features. Starting from the middle of the diagram, the frontier states (degenerated orbitals) could hold multiple electrons and display continuous peaks separated by quantized charging energy, with four continuous peaks resolved from this specific MTC sample. With ca. 29 Durene-DT ligands in the monolayer, multiple LUMO states are accessible for electrochemical reduction or optical excitation at the same energy states.

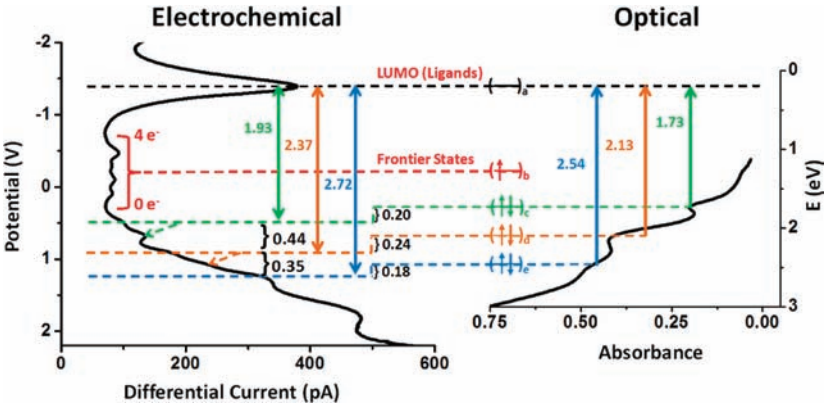

Figure 8. Energy diagram that correlates optical and electrochemical features. The oxidation scan (left) and absorbance spectrum (right) are aligned based on the energy stated shown in the middle. The undetermined degeneracy of those states are denoted c, d, and e.

Note this is different from the charging of core energy states, which requires charging energy for each additional electron transfer activity.

With the distinct LUMO as reference point (mainly contributed from Durene-DT ligands), electrochemical and optical transitions are correlated. The first three optical absorption bands at 1.73, 2.13, and 2.54 eV are matched with corresponding electrochemical peaks as indicated. Note the first of the two ET peaks in each energy state (corresponding to 1.73 and 2.13 optical bands) is used in the comparison. The second ones are indicated by the arrow, requiring additional charging energy compared to the first ones. The average differences between measured optical and electrochemical transitions (0.2 V) are approximately equivalent to the measured charging energy (0.19 V). The high background signal at high potentials and potential structure/composition changes of MTC at high charge states in electrochemistry prohibit the precise correlation of the 3.50 eV optical band, as well as the degeneracy of those energy states.

The optical band gap is extrapolated to be ca. 0.88 eV from the absorbance spectrum, but varies from sample to sample and is not as well-defined as the other bands. With 0−4 electrons filling the frontier energy states, the Fermi level will shift accordingly, which will cause the absorption band gap to vary. Indeed, the rest potential of the sample used here is ~0.09 V with Ag/AgCl wire as quasi reference electrode. Typical rest potentials vary from −0.05 V to +0.10 V for different batches of Au_{130} MTC samples. For an ideal neutral MTC sample, the HOMO−LUMO gap is predicted to be 0.74 V from electrochemistry, calculated from the gap between the LUMO peak and the last charging peak of the HOMO (0.93 V) with one charging energy value (0.19 V) subtracted.

CONCLUSIONS

In summary, interesting energetics is observed from a new type of molecular gold cluster protected by mixed monothiol ligand and dithiol ligand. The molecular ion at ca. 34.8 kDa was detected by MALDI-MS. The mole ration of Au:Durene-DT/PhC2S was determined by TGA and NMR techniques. The Au−S bond formation and charge states were studied by XPS and IR spectroscopy. The average composition of the Au MTCs is determined as $Au_{130}(Durene\text{-}DT)_{29}(PhC2S)_{22}$ at ±1−2 resolution. The MTCs display multiple discrete absorption bands, originated from core−ligand charge delocalization. Quantized double charging behaviors are observed at lower potentials in voltammetric measurements. Ligand reaction is observed at higher potential ranges. An energy diagram has been proposed to correlate the optical and electrochemical energetics of this molecular nanocluster. The interesting energetics is attributed to the unique structural constraints imposed by the dithiolate ligand on the interfacial bonding structures at the gold core surface that demand further investigation.

ASSOCIATED CONTENT

Supporting Information. Synthesis and purification of the Au MTCs, MS spectra, NMR spectra, HPLC separation data, emission and excitation spectra, TGA data, XPS data and additional electrochemistry data. This material is available free of charge via the Internet at http://pubs.acs.org.

AUTHOR INFORMATION

Corresponding Author
glwang@gsu.edu

ACKNOWLEDGMENT

We thank Chun Huang (Department of Chemistry and Biochemistry, Georgia Institute of Technology) for his generous help of TGA measurements. We thank Dr. Markus W. Germann for access of NMR spectrometer for DOSY measurement. The Nanotechnology Research Center at Georgia Institute of Technology is acknowledged for XPS measurements. The start-up supports at Georgia State University is acknowledged. This material is also based upon work supported by the National Science Foundation under Grant No. 1059022.

REFERENCES

(1) Daniel, M.-C.; Astruc, D. *Chem. Rev.* **2004**, *104*, 293.
(2) Murray, R. W. *Chem. Rev.* **2008**, *108*, 2688.
(3) Sardar, R.; Funston, A. M.; Mulvaney, P.; Murray, R. W. *Langmuir* **2009**, *25*, 13840.
(4) Zhu, Y.; Qian, H.; Zhu, M.; Jin, R. *Adv. Mater.* **2010**, *22*, 1915.
(5) Han, G.; Ghosh, P.; Rotello, V. M. *Nanomedicine* **2007**, *2*, 113.
(6) Giljohann, D. A.; Seferos, D. S.; Daniel, W. L.; Massich, M. D.; Patel, P. C.; Mirkin, C. A. *Angew. Chem., Int. Ed.* **2010**, *49*, 3280.
(7) Jadzinsky, P. D.; Calero, G.; Ackerson, C. J.; Bushnell, D. A.; Kornberg, R. D. *Science* **2007**, *318*, 430.

(8) Heaven, M. W.; Dass, A.; White, P. S.; Holt, K. M.; Murray, R. W. *J. Am. Chem. Soc.* **2008**, *130*, 3754.
(9) Zhu, M.; Aikens, C. M.; Hollander, F. J.; Schatz, G. C.; Jin, R. *J. Am. Chem. Soc.* **2008**, *130*, 5883.
(10) Qian, H.; Eckenhoff, W. T.; Zhu, Y.; Pintauer, T.; Jin, R. *J. Am. Chem. Soc.* **2010**, *132*, 8280.
(11) Zhu, M.; Eckenhoff, W. T.; Pintauer, T.; Jin, R. *J. Phys. Chem. C* **2008**, *112*, 14221.
(12) Jiang, D.-e.; Tiago, M. L.; Luo, W.; Dai, S. *J. Am. Chem. Soc.* **2008**, *130*, 2777.
(13) Jiang, D.-e.; Luo, W.; Tiago, M. L.; Dai, S. *J. Phys. Chem. C* **2008**, *112*, 13905.
(14) Hakkinen, H.; Walter, M.; Gronbeck, H. *J. Phys. Chem. B* **2006**, *110*, 9927.
(15) Akola, J.; Walter, M.; Whetten, R. L.; Hakkinen, H.; Gronbeck, H. *J. Am. Chem. Soc.* **2008**, *130*, 3756.
(16) Jiang, D.-e.; Chen, W.; Whetten, R. L.; Chen, Z. *J. Phys. Chem. C* **2009**, *113*, 16983.
(17) Walter, M.; Akola, J.; Lopez-Acevedo, O.; Jadzinsky, P. D.; Calero, G.; Ackerson, C. J.; Whetten, R. L.; Gronbeck, H.; Hakkinen, H. *Proc. Natl. Acad. Sci. U.S.A.* **2008**, *105*, 9157.
(18) Tang, Z.; Xu, B.; Wu, B.; Germann, M. W.; Wang, G. *J. Am. Chem. Soc.* **2010**, *132*, 3367.
(19) Tang, Z.; Xu, B.; Wu, B.; Robinson, D. A.; Bokossa, N.; Wang, G. *Langmuir* **2011**, *27*, 2989.
(20) Zhang, S.; Leem, G.; Srisombat, L.-o.; Lee, T. R. *J. Am. Chem. Soc.* **2008**, *130*, 113.
(21) Hou, W.; Dasog, M.; Scott, R. W. J. *Langmuir* **2009**, *25*, 12954.
(22) Garg, N.; Lee, T. R. *Langmuir* **1998**, *14*, 3815.
(23) Wu, Z.; Lanni, E.; Chen, W.; Bier, M. E.; Ly, D.; Jin, R. *J. Am. Chem. Soc.* **2009**, *131*, 16672.
(24) Srisombat, L. O.; Park, J. S.; Zhang, S.; Lee, T. R. *Langmuir* **2008**, *24*, 7750.
(25) Li, Z.; Jin, R.; Mirkin, C. A.; Letsinger, R. L. *Nucleic Acids Res.* **2002**, *30*, 1558.
(26) Krpetic, Z.; Nativo, P.; Porta, F.; Brust, M. *Bioconjugate Chem.* **2009**, *20*, 619.
(27) Jackson, A. M.; Myerson, J. W.; Stellacci, F. *Nat. Mater.* **2004**, *3*, 330.
(28) DeVries, G. A.; Brunnbauer, M.; Hu, Y.; Jackson, A. M.; Long, B.; Neltner, B. T.; Uzun, O.; Wunsch, B. H.; Stellacci, F. *Science* **2007**, *315*, 358.
(29) Lee, T. R.; Friedman, J. M.; Garg, N. *Langmuir* **2000**, *16*, 4266.
(30) Garg, N.; Lee, T. R. *Langmuir* **1998**, *14*, 3815.
(31) Brust, M.; Walker, M.; Bethell, D.; Schiffrin, D. J.; Whyman, R. *J. Chem. Soc., Chem. Comm* **1994**, 801.
(32) Templeton, A. C.; Hostetler, M. J.; Kraft, C. T.; Murray, R. W. *J. Am. Chem. Soc.* **1998**, *120*, 1906.
(33) Wu, Z.; Suhan, J.; Jin, R. *J. Mater. Chem.* **2009**, *19*, 622.
(34) Dharmaratne, A. C.; Krick, T.; Dass, A. *J. Am. Chem. Soc.* **2009**, *131*, 13604.
(35) Donkers, R. L.; Lee, D.; Murray, R. W. *Langmuir* **2004**, *20*, 1945.
(36) Lee, D.; Donkers, R. L.; Wang, G.; Harper, A. S.; Murray, R. W. *J. Am. Chem. Soc.* **2004**, *126*, 6193.
(37) Negishi, Y.; Nobusada, K.; Tsukuda, T. *J. Am. Chem. Soc.* **2005**, *127*, 5261.
(38) Parker, J. F.; Weaver, J. E. F.; McCallum, F.; Fields-Zinna, C. A.; Murray, R. W. *Langmuir* **2010**, *26*, 13650.
(39) Qian, H.; Zhu, Y.; Jin, R. *ACS Nano* **2009**, *3*, 3795.
(40) Toikkanen, O.; Ruiz, V.; Ronnholm, G.; Kalkkinen, N.; Liljeroth, P.; Quinn, B. M. *J. Am. Chem. Soc.* **2008**, *130*, 11049.
(41) Qian, H.; Zhu, M.; Andersen, U. N.; Jin, R. *J. Phys. Chem. A* **2009**, *113*, 4281.
(42) Qian, H.; Jin, R. *Nano Lett.* **2009**, *9*, 4083.
(43) Dass, A.; Stevenson, A.; Dubay, G. R.; Tracy, J. B.; Murray, R. W. *J. Am. Chem. Soc.* **2008**, *130*, 5940.
(44) Qian, H.; Zhu, Y.; Jin, R. *J. Am. Chem. Soc.* **2010**, *132*, 4583.
(45) Negishi, Y.; Iwai, T.; Ide, M. *J. Chem. Soc., Chem. Comm* **2010**, *46*, 4713.
(46) Jimenez, V. L.; Leopold, M. C.; Mazzitelli, C.; Jorgenson, J. W.; Murray, R. W. *Anal. Chem.* **2003**, *75*, 199.
(47) Hostetler, M. J.; Wingate, J. E.; Zhong, C. J.; Harris, J. E.; Vachet, R. W.; Clark, M. R.; Londono, J. D.; Green, S. J.; Stokes, J. J.; Wignall, G. D.; Glish, G. L.; Porter, M. D.; Evans, N. D.; Murray, R. W. *Langmuir* **1998**, *14*, 17.
(48) Guo, R.; Song, Y.; Wang, G.; Murray, R. W. *J. Am. Chem. Soc.* **2005**, *127*, 2752.
(49) Song, Y.; Murray, R. W. *J. Am. Chem. Soc.* **2002**, *124*, 7096.
(50) Parker, J. F.; Choi, J. P.; Wang, W.; Murray, R. W. *J. Phys. Chem. C.* **2008**, *112*, 13976.
(51) Donkers, R. L.; Lee, D.; Murray, R. W. *Langmuir* **2004**, *20*, 1945.
(52) Pregosin, P. S.; Kumar, P. G. A.; Fernandez, I. *Chem. Rev.* **2005**, *105*, 2977.
(53) Kohlmann, O.; Steinmetz, W. E.; Mao, X. A.; Wuelfing, W. P.; Templeton, A. C.; Murray, R. W.; Johnson, C. S. *J. Phys. Chem. B* **2001**, *105*, 8801.
(54) Canzi, G.; Mrse, A. A.; Kubiak, C. P. *J. Phys. Chem. C* **2011**, *115*, 7972.
(55) Link, S.; Beeby, A.; FitzGerald, S.; El-Sayed, M. A.; Schaaff, T. G.; Whetten, R. L. *J. Phys. Chem. B* **2002**, *106*, 3410.
(56) Wang, G.; Huang, T.; Murray, R. W.; Menard, L.; Nuzzo, R. G. *J. Am. Chem. Soc.* **2005**, *127*, 812.
(57) Cheng, P. P. H.; Silvester, D.; Wang, G.; Kalyuzhny, G.; Douglas, A.; Murray, R. W. *J. Phys. Chem. B* **2006**, *110*, 4637.
(58) Huang, T.; Murray, R. W. *J. Phys. Chem. B* **2001**, *105*, 12498.
(59) Yam, V. W.-W.; Cheng, E. C.-C. *Chem. Soc. Rev.* **2008**, *37*, 1806.
(60) Fackler, J. P. *Inorg. Chem.* **2002**, *41*, 6959.
(61) Wang, G.; Guo, R.; Kalyuzhny, G.; Choi, J. P.; Murray, R. W. *J. Phys. Chem. B* **2006**, *110*, 20282.
(62) Wu, Z.; Jin, R. *Nano Lett.* **2010**, *10*, 2568.
(63) Bain, C. D.; Badia, H. A.; Whitesides, G. M. *Langmuir* **1989**, *5*, 723.
(64) Bourg, M.-C.; Badia, A.; Lennox, R. B. *J. Phys. Chem. B* **2000**, *104*, 6562.
(65) Shon, Y. S.; Gross, S. M.; Dawson, B.; Porter, M.; Murray, R. W. *Langmuir* **2000**, *16*, 6555.
(66) Quinn, B. M.; Liljeroth, P.; Ruiz, V.; Laaksonen, T.; Kontturi, K. *J. Am. Chem. Soc.* **2003**, *125*, 6644.
(67) Hicks, J. F.; Miles, D. T.; Murray, R. W. *J. Am. Chem. Soc.* **2002**, *124*, 13322.
(68) Balasubramanian, R.; Guo, R.; Mills, A. J.; Murray, R. W. *J. Am. Chem. Soc.* **2005**, *127*, 8126.
(69) Laaksonen, T.; Ruiz, V.; Lijeroth, P.; Quinn, B. M. *Chem. Soc. Rev.* **2008**, *37*, 1836.
(70) Gilbert, B. C.; Laue, H. A. H.; Norman, R. O. C.; Sealy, R. C. *J. Chem. Soc., Perkin Trans. 2* **1975**, 892.
(71) Mason, R. P.; Chignell, C. F. *Pharmacological Rev.* **1982**, *33*, 189.
(72) Moses, P. R.; Chambers, J. Q.; Sutherland, J. O.; Williams, D. R. *J. Electrochem. Soc.* **1975**, *122*, 608.
(73) Aarons, L. J.; Adam, F. C. *Can. J. Chem.* **1972**, *50*, 1390.
(74) Garcia-Morales, V.; Mafe, S. *J. Phys. Chem. C* **2007**, *111*, 7242.